Halo observations provide evidence of airborne cubic ice in the Earth's atmosphere

Marko Riikonen, Mika Sillanpää, Leena Virta, Daniel Sullivan, Jarmo Moilanen, and Ismo Luukkonen

An ice crystal halo display that contains several previously unknown halo phenomena was observed in Northern Chile. Analysis of computer simulations of the halos demonstrates that most of the new halo arcs in the display can be explained by the presence of airborne and preferentially oriented crystals of cubic ice. These observations therefore provide evidence of the existence of the cubic phase of ice in the Earth's atmosphere. © 2000 Optical Society of America

OCIS codes: 010.1290, 010.2940, 290.5850.

1. Introduction

Atmospheric halos are rings and arcs of light in the sky. They are the result of reflection and refraction of sunlight or moonlight by ice crystals in the atmosphere, usually in cirrus or cirrostratus clouds in the upper troposphere.[1] All well-documented halos so far have been caused by crystals of hexagonal ice (ice Ih). The most common form of halo-making crystals is a hexagonal cylinder or plate with basal faces at their ends, which gives rise to the 22° and 46° circular halos and their associated arcs. Less common are the hexagonal crystals with developed pyramidal $\{1,0, -1,1\}$ faces having a pyramid apex angle of 56.1°. These crystals cause circular halos with radii of 9°, 18°, 20°, 23°, 24°, and 35°, as well as their associated arcs.[1,2] There is also some evidence of the presence of nontypical pyramidal crystals with high pyramid apex angles between 170° and 176°. These crystals are believed to give rise to elliptical halos: rare transient phenomena observed close to the position of the Sun in the sky.[3]

The possibility of the existence of ice with a cubic crystalline structure (ice Ic) in the Earth's atmosphere has been discussed in several papers.[4–9] One way to analyze the particle content of the atmosphere is to study scattering produced by these particles, that is, to study halos. In 1981 Whalley[4] proposed that the historic reports of the occurrence of a rare circular halo of 26–29° radius known as Scheiner's halo, for which there was no photographic evidence, provides evidence of the existence of ice Ic in the atmosphere. As a possible cause of this phenomenon, Whalley suggested halo formation by the octahedral form of ice Ic crystals, the halo-making pairs of faces making an angle of 70.5° with each other. Given the fact that the density and hence the refractive index of ice Ic and ice Ih are almost equal,[5,10–12] randomly oriented ice Ic octahedrals would produce a circular halo around the Sun of 28° radius.

Apart from Whalley's claim, no further evidence of naturally occurring airborne ice Ic is known. In laboratory experiments, ice Ic is produced when water vapor condenses on a substrate whose temperature is around 180 K. If the temperature is too low, amorphous ice would be formed.[4,5] It has been suggested that water droplets are able to freeze to ice Ic in some amounts at approximately 230 K.[4,5] It is also possible that the crystals grow directly from the vapor phase. Ice Ic would probably crystallize in a similar octahedral form as diamond, inasmuch as they both belong to the $m3m$ crystal class.

Here we present photographs and computer simulations of a halo display observed on 27 and 28 November 1997, from the foot of the persistently steaming Lascar volcano (23°22′S 68°34′W) in the northern Chilean altiplano. Apart from a number of prominent halos that are due to pyramidal ice Ih crystals, the display definitely contained several, previously undocumented halo phenomena, most of which can be satisfactorily explained by octahedral ice Ic crystals falling in the air in a preferential ori-

M. Riikonen, L. Virta, D. Sullivan, J. Moilanen, and I. Luukkonen are with the Ursa Astronomical Association, Raatimiehen-katu 3, 00140 Helsinki, Finland. M. Sillanpää (mika.sillanpaa@iki.fi) is with the Low Temperature Laboratory, Helsinki University of Technology, P.O. Box 2200, 02015 Espoo, Finland.

(a) $h = 42°$ **(b)** $h = 27°$
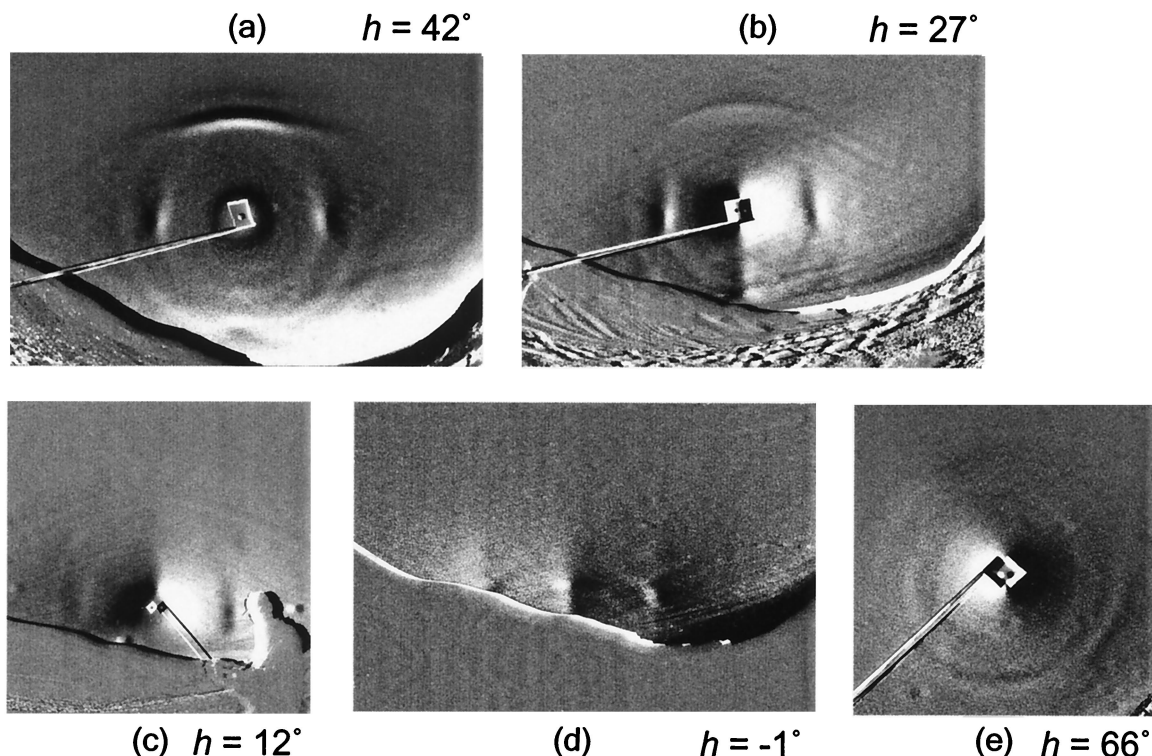
(c) $h = 12°$ **(d)** $h = -1°$ **(e)** $h = 66°$

Fig. 1. Photographs of the display at solar elevation h of approximately (a) 42°, (b) 27, (c) 12°, (d) −1°, (e) 66°. The photographs in (a)–(d) were taken on 27 November; the photograph in 1(e) is from the next day. The photograph in (e) is slanted, with the horizon at the lower right-hand corner. Image contrast was enhanced by digital image processing to compensate for the reduced resolution in reproduction. We processed the images by first applying an embossed filter and then by increasing the black-and-white image contrast to an optimal value. The processed and the original images of the halo display can be viewed at http://www.iki.fi/mika.sillanpaa/ichalos.

entation. This conclusion is further supported by the unusually low temperatures measured at the upper part of the troposphere close to the observation site.

2. Observed Halo Display

The halo display was first noticed on 27 November, 16:20 local time (19:20 UT). It appeared to be caused by a thin, uniform high cloud that was almost invisible except close to the horizon. The display lasted until sunset. The following morning the display was again present in the sky, the appearance being strikingly similar to that observed the previous evening. As the Sun rose, the halo complex was observed to undergo changes in the reverse direction to those observed with the setting of the Sun the previous evening. The display lasted until afternoon, although by midday it had already started to lose its intensity.

The range in solar elevations covered photographically during the two days was from approximately −1° to 66°. Given in chronological order, we present five contrast-enhanced photographs [Figs. 1(a)–1(e)] from the approximately 100 photographs that were taken of the phenomena, distributed evenly in solar elevation, showing the essential stages of the display. For Figs. 1(a)–1(c) the time each photograph was taken was recorded within an interval of 10–30 min. There are no time recordings for Figs. 1(d) and 1(e),

and the estimate of solar elevation for these photographs is based on the solar elevation used in the simulation that gives the best match with each photograph. The solar elevations used in the simulation of Figs. 1(a)–1(c) agree with the time recordings of the corresponding photographs to within ±1.5°.

3. Simulation of the Display

Our halo simulation algorithm is similar to that of Pattloch and Tränkle[13] and of Tape.[1] The simulations do not take into account scattering caused by the atmosphere or the increased optical depth of the ice cloud near the horizon, both of which would tend to weaken and diffuse the halos.[14] Hence, weak halos predicted by the simulations to be located close to the horizon may be invisible in the observed display.

In the simulations five different crystal populations were used; three populations of ice Ic crystals denoted as C-I, C-II, and C-III and two populations of pyramidal ice Ih crystals denoted as H-I and H-II. Of the ice Ic crystal populations, the first, C-I, contains crystals with one octahedral face horizontally oriented and with strong crystal tilting angles (the variance in zenith angle of the crystallographic c axis) and one corner with a pronounced truncation [Fig. 2(a)]. Crystals of the second population, C-II, are randomly oriented with minimal truncation of two crystal corners [Fig. 2(b)]. The analog of the orientation pattern of crystals in population C-I has never
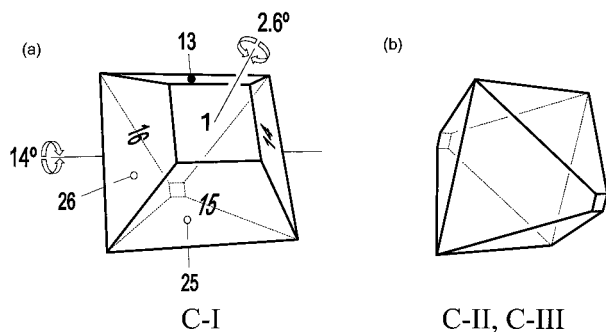
Fig. 2. Crystals of cubic ice to simulate the halo display: (a) population C-I showing the orientation and the numbering of crystal faces and (b) populations C-II and C-III. Crystals in population C-II are randomly oriented, in C-III they are not. C-III was used only for the simulation of Fig. 1(d).
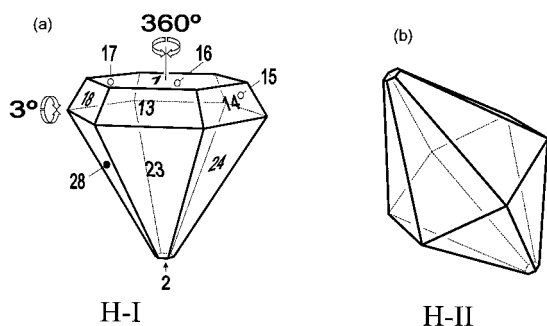

Fig. 3. Pyramidal crystals of hexagonal ice for simulation of the halo display: (a) population H-I showing the orientation and the numbering of the crystal faces and (b) population H-II. Crystals in the H-II population are almost randomly oriented with strong deviation of the c-axis orientation.

before been documented for pyramidal Ih crystals. However, the significantly dissimilar habit of cubic ice crystals could permit them to maintain such an orientation. In the simulation of Fig. 1(c), one additional ice Ic population, C-III, is invoked, the crystals having a vertically oriented c axis, strong crystal tilting angles, and, like C-II, minimal truncation of two pyramidal ends. A crystal of ice Ih population H-I, oriented with a vertical c axis, with small crystal tilting angles and pronounced pyramidal truncation, is shown in Fig. 3(a). The second Ih population, H-II, contains almost randomly oriented crystals

Table 2. Ray Paths for the Halos and Arcs that Appear in the Simulations[a]

Population	Halo Type	Ray Path(s)
H-I	18° parhelia (18P)	13–25
	20° upper parhelion (20UP)	13–16
	20° lower parhelion (20LP)	23–26
	23° upper parhelion (23UP)	1–23
	23° lower parhelion (23LP)*	13–2
	35° upper parhelion (35UP)	13–15
	35° lower parhelion (35LP)	23–25
H-II	18° halo (18H)	13–25
	20° halo (20H)	13–16
C-I	28Ca*	13–15, 13–24
	28Cb*	14–25, 23–25
	28Cc*	14–16, 16–23, 23–14
	28Cd*	26–24, 24–15, 15–26
	19Ca*	1–26
	19Cb*	1–23, 23–1
	19Cc*	1–25
C-II	28° halo (28H)*	13–15, 13–24
C-III	28Ce*	13–15

[a]Figures 2 and 3 provide the numbers for the ice Ih (H) and ice Ic (C) crystal faces. The abbreviated halo names are within parentheses. The first number in the coding of the ice Ic halos (19, 28) refers to the radius of the circular halo with which it is associated. The two ray paths for arc 19Cb actually form two different halo arcs, but the strong tilting angles of the crystals in the simulations cause these arcs to merge. Population C-III has been invoked only for the simulation of Fig. 1(d) (−1° solar elevation). Halos and arcs for which we do not know of earlier photographic documentation are marked by an asterisk.

with strong crystal tilting angles and minimal pyramidal truncation [Fig. 3(b)]. Note that H-I and H-II lack prism faces. More specific parameters for the simulations are listed in Table 1.

Using the truncated octahedral model of ice Ic [Fig. 2(a)] creates two distinct halo angles. Paths through faces 1–23 have a minimum deviation of 19°, whereas paths through faces 13–15 and 13–24 both have minimum deviation of 28°. A nontruncated ice Ic crystal has only the 28° minimum deviation angle. In ice Ih crystals, as in Fig. 3, four different refractive angles occur. The ray paths for these are 13–25, 13–16, 1–23, and 13–15, with corresponding minimum deviations of 18°, 20°, 23°, and 35°.

Solar angular distances of most of the halos and

Table 1. Parameters for Simulations[a]

Population	H-I	H-II	C-I	C-II	C-III
Number of rays	3500 (2000)	2500 (3000)	5000 (2000)	4500 (2000)	2000
c-axis angle/var.(°)	0/3 (0/3.4)	0/25 (0/30)	54.75/14	Random	0/15
Rotation around c-axis average/var.(°)	Random	Random	0/2.6	Random	0/5
Trunc./var for faces 13 . . . 8	0.81/0.2 (0.81/0.05)	0.1/0.1	0.4/0.2 (0.3/0.2)	0/0.05	0.05/0.05
Trunc./var for faces 23 . . . 8	0.2/0.2 (0.18/0.05)	0.1/0.1	0/0.2	0/0.05	0.05/0.05

[a]Var is the variance of the Gaussian distribution. The c axis refers to the crystallographic axis. In the hexagonal system, it is the crystal's principal axis. The c-axis angle is the average angle relative to the vertical direction. The zero rotation angle around the c axis means that the tilting direction of the c axis is perpendicular to one side face. Truncation of a pyramidal end is defined as $(H - h)/H$, where H and h are the nontruncated and truncated height of the pyramid, respectively (for example, a crystal with a truncation of zero is a complete crystal with no truncation of the crystal ends). The values within parentheses were used in Fig. 4(d).
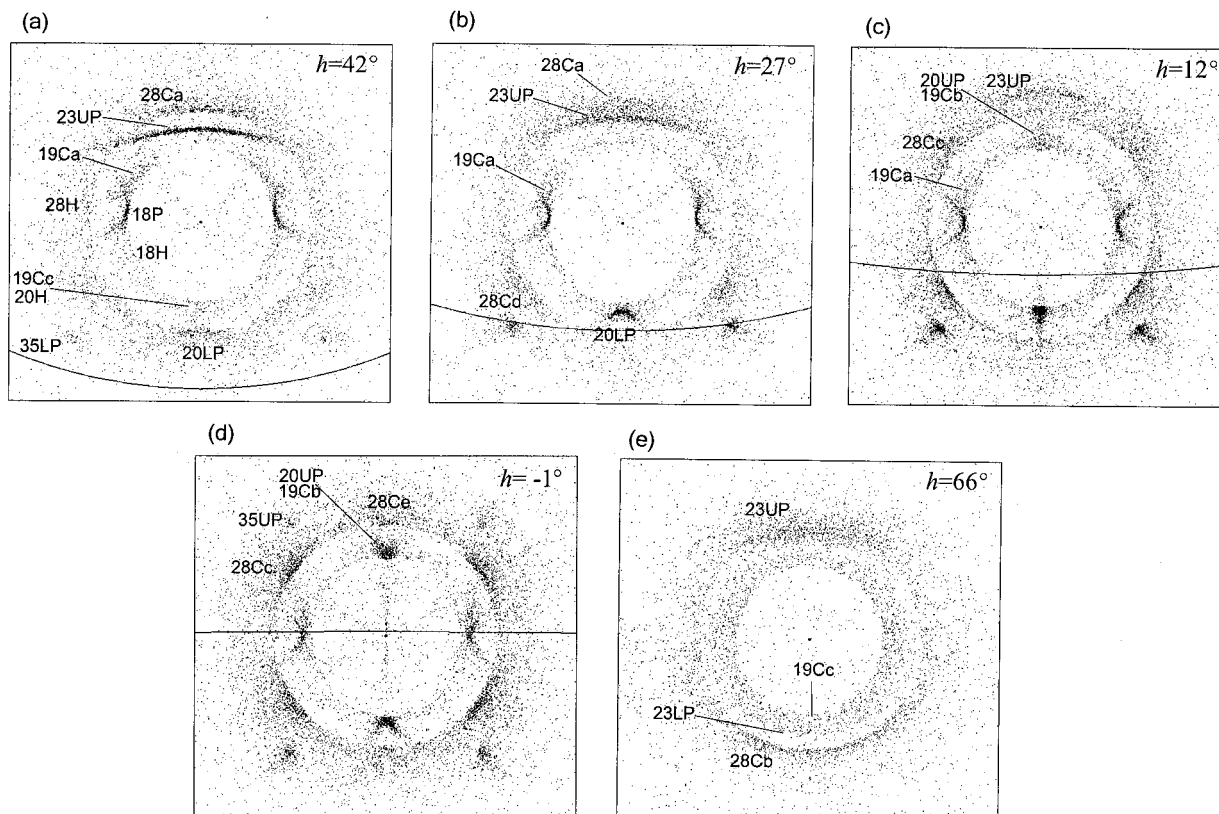
Fig. 4. Outcome of simulations at the following solar elevations h: (a) 42°, (b) 27, (c) 12°, (d) −1°, (e) 66°. The horizon is marked by a solid curve (only arcs above the horizon are shown in the photographs).

arcs in the display were measured for different solar elevations. They were obtained from the photographs by careful comparisons with a photograph of a star field taken with the same lens. The agreement between measured and calculated values of radii of the circular halos was good in each case. Seven measurements of the inner edge of the circular halo with a supposed angular distance of 28° resulted in a mean value of 28.4° ± 0.9°.

The names for halos used in this paper are as follows: no names for the previously unobserved or unpredicted arcs; for arcs arising from Ih crystals with vertically oriented c axes (H-II) we use the term parhelia after Tape.[1] The circular halos that are due to random orientation are referred to as such. Ray paths for all the simulated halos are listed in Table 2.

4. Analysis of the Phenomena by Computer Simulations

Figure 1(a) presents the photographed halo display, soon after detection, at a solar elevation of approximately 42°. In the simulation represented in Fig. 4(a), the previously undocumented halos are labeled 28Ca, 19Ca, and 19Cc. Arc 28Ca is clearly visible in the photo. Both 19Ca arcs are not as clear because, in the simulation as well as in the photograph, they overlap with the ice Ih 18° circular halo (18H). This gives an impression of the 18° circular halo being

slightly brighter upward of the 18° parhelia (18P). There is a slight discrepancy between the positioning of the observed and the simulated effects of 19Ca; the simulated 19Ca arc seems to be located slightly higher than the observed arc. According to simulations, arc 19Cc alone is a rather faint effect and consequently is unlikely to explain the halo spot seen in the photograph at the corresponding location. This particular location is also illuminated in the simulation by the ray path of the circular 20° halo (20H) that is due to ice Ih, but the resultant effect is still much fainter than in the photograph, leaving some uncertainty in its identification. The 28° halo, marked 28H in the simulation, shows up faintly in Fig. 1(a) to the left and to the right of the Sun.

In Fig. 1(b), at a solar elevation of approximately 27°, the display has not changed considerably from the stage considered in Fig. 1(a). The simulation in Fig. 4(b) predicts one new halo arc, 28Cd, which is seen in Fig. 1(b) as the more intense part of the circular 28° halo close to the horizon. A feature not visible in the simulation is the pillarlike brightening below the Sun, which is noticeable in several photos, with a varying length and is clearly part of a Sun pillar caused by a greater density in cloud material.

Figure 1(c) presents a stage of the display at a solar elevation of approximately 12°. The corresponding simulation in Fig. 4(c) was created by use of the same crystal populations as in Figs. 4(a) and 4(b). Be-

cause of the change in solar elevation, the resultant intensity pattern is now markedly different from previous simulations. New ice Ic halos seen in the simulation are arcs 28Cc and 19Cb. Arc 28Cc is clear in the photo, but 19Cb is occluded by another halo, the 20° upper parhelion (20UP) above it.

In Fig. 1(d), at a solar elevation of approximately −1°, arc 19Cb overlaps the 20° upper parhelion, as is shown by the simulation in Fig. 4(d). An interesting feature in Fig. 1(d) is the faint brightening toward the top of the circular 28° halo. Simulations that employ the previously used parameters do not demonstrate this effect. By introducing an additional population (C-III) of crystals of cubic ice (see Table 1), falling with their *c* axes poorly oriented with the vertical, this phenomenon appears and is labeled 28Ce in Fig. 4(d). This suggests that there was a swiftly passing population of differently oriented cubic ice crystals. At higher solar elevations [Figs. 1(a)–1(e)] this crystal population would produce arcs that are not seen in the photos.

Figure 1(e) presents the display from the next day at a solar elevation of approximately 66°. Simulation parameters have been changed slightly from the previous day (see Table 1 for details). The most conspicuous halo in Fig. 1(e) is the arc farthest below the Sun, labeled 28Cb in Fig. 4(e), which represents the corresponding simulation. As shown in Fig. 1(e) a broad circular halo appears at approximately 20° from the Sun. According to the simulation, from its lower parts it is caused by several halos and arcs: the 20° halo, the 18° halo, the 23° lower parhelion (23LP), and arc 19Cc. Photographic measurements from the solar vertical of the outer edge of this broad halo confirmed it to be 24.5° from the Sun. This matches the theoretical location of the 23° lower parhelion's outer edge at this solar elevation. This seems to be the first observation of the recently predicted 23° lower parhelion.[2] The inner edge of the broad haloing below the Sun is too faint to be measured reliably.

5. Discussion

The simulations show all the different halo arcs that crystals, shaped and oriented as in Fig. 2(a), would produce at the photographed solar elevations. These arcs can indeed be seen in the photographs, although identification of arcs 19Cb and 19Cc is disturbed by halo arcs from the ice Ih. In addition to the solar elevations discussed in this paper we also simulated other solar elevations for which photographs were available with the same crystal parameters but without invoking population C-III, and found that the resultant intensity patterns were a good match with the corresponding photographs. At a solar elevation of around 3°, however, an additional halo arc is visible in our photographs, located at 11–12° above the solar vertical. This arc, which does not appear in our simulations, matches the recently discovered arc of Moilanen that has been observed so far only at low solar elevations.[15]

Prior to invoking ice Ic crystals in our simulations,
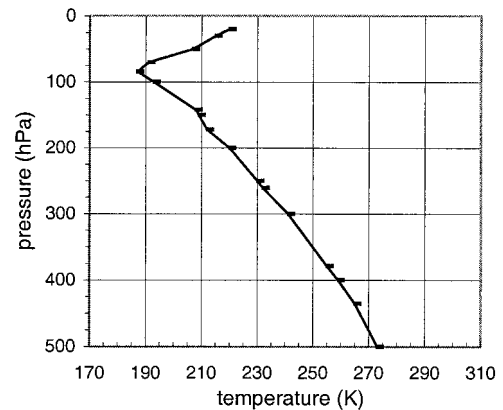

Fig. 5. Atmospheric temperature recordings below 273 K for Antofagasta on 28 November 1997 at 09:00 local time.

attempts were made to simulate the display by use of hexagonal ice crystals with pyramidal apex angles that differ from the common 56.14°. We found that pyramidal crystal pyramid apex angles of 39°, 96°, 109°, and 142° produce circular halos of 27–29° radii and associated arcs. However, the simulated intensity patterns produced by these crystals could not be matched with the observed display. Hexagonal crystals have more possible ray paths through the crystal than the form used for cubic ice, which results in several halos and arcs that were not observed in the display.

Weinheimer and Knight[6] proposed an alternative explanation for the 28° halo in 1987. They suggested that the 28° halo could be caused by ray paths through the basal faces of the initial form of hexagonal polycrystal. According to this hypothesis the 28° halo would be visible only for a short period of time before the crystals grew into twin crystals. However, in the display observed by us the crystal populations seem to remain almost unchanged for 24 h. Although simulations with the polycrystal would still be worth making, it is as yet beyond the scope of our algorithm.

The resemblance between the shapes of crystals in the ice Ic and the ice Ih populations (Figs. 2 and 3) is noticeable. The ice Ih crystals seem to lack prism faces, as neither 22° nor 46° halos are seen. This is an extraordinary situation. Inasmuch as ice Ic is metastable relative to ice Ih, it may be possible that the ice Ih crystals in this halo display have developed from the Ic crystals. Alternatively, both ice Ih and ice Ic crystals may have formed separately from the frozen water droplets. Pyramidal ice Ih crystals are traditionally thought to originate from frozen water droplets.[16]

An upper air sounding (Fig. 5) is available from 28 November from Antofagasta, a town located 250 km west from the observation point. A minimum temperature of 187 K was recorded at the 84.3-hPa level. The wind at that level was from the west, at a speed of 16 m/s. With the wind 16 m/s at 84.3 hPa blowing toward the observation area, it would take approximately 4–5 h for air to reach the observation

site. As the radiosonde was released at 09:00 local time, these data are representative of our observations between 13:00 and 14:00 local time. The display was still faintly visible at that time. If the moisture that produced the halos was the layer around 84.3 hPa in the sounding, these low temperatures in the upper troposphere would be in good agreement with the low temperature requirement for cubic ice formation.

Although direct evidence of atmospheric ice Ic is still missing, we believe that ice Ic crystals have been responsible for most of the new arcs observed in the display. The overall agreement between the photos and simulations is good, although there are still minor discrepancies in the details. Additional photographic records of these halos in the future are hoped for. Should further observations be made of these phenomena, they will possibly recur in connection with halos caused by pyramidal ice Ih crystals. Three other displays with 18° parhelia and a 23° upper parhelion were observed at Lascar within one month of the display described in this paper, perhaps suggesting a regular presence of pyramidal Ih crystals in the area. Crystal samples, taken during low-level pyramidal ice Ih halo displays that occur in cold polar climates, might also reveal the presence of some cubic ice crystals among ordinary hexagonal crystals.

References

1. W. Tape, *Atmospheric Halos*, Vol. 64 of Antarctic Research Series, (American Geophysical Union, Washington, D.C, 1994).
2. M. Pekkola, M. Riikonen, J. Ruoskanen, and J. Moilanen, "Halo arcs from airborne, pyramidal ice crystals falling with their *c* axes in vertical orientation," Appl. Opt. **37,** 1435–1440 (1998).
3. M. Sillanpää, J. Moilanen, M. Pekkola, M. Penttinen, and J. Piikki, "Unusual pyramidal ice in the atmosphere as the origin of elliptical halos," Appl. Opt. **38,** 5089–5095 (1999).
4. E. Whalley, "Scheiner's halo: evidence for ice Ic in the atmosphere," Science **211,** 389–390 (1981).
5. E. Whalley, "Cubic ice in nature," J. Phys. Chem. **87,** 4174–4179 (1983).
6. A. J. Weinheimer and C. A. Knight, "Scheiner's halo: cubic ice or polycrystalline hexagonal ice?," J. Atmos. Sci. **44,** 3304–3308 (1987).
7. N. Sato and K. Kikuchi, "Crystal structure of typical snow crystals of low temperature type," J. Meteorol. Soc. Jpn. **60,** 521–528 (1989).
8. R. P. Turco, "Noctilucent clouds: simulation studies of their genesis, properties and global influences," Planet. Space Sci. **30,** 1147–1191 (1982).
9. E. Mayer and A. Hallbrucker, "Cubic ice from liquid water," Nature (London) **325,** 601–602 (1987).
10. P. V. Hobbs, *Ice physics* (Clarendon, Oxford, 1974).
11. G. P. Arnold, E. D. Finch, S. W. Rabideau, and R. G. Wenzel, "Neutron-diffraction study of ice polymorphs, III. Ice Ic," J. Chem. Phys. **49,** 4365–4369 (1968).
12. M. Kurnai, "Hexagonal and cubic ice at low temperatures," J. Glaciol. **7,** 95–108 (1968).
13. F. Pattloch and E. Tränkle, "Monte Carlo simulation and analysis of halo phenomena," J. Opt. Soc. Am. A **1,** 520–526 (1984).
14. S. D. Gedzelman, "Simulating rainbows and halos in color," Appl. Opt. **33,** 4607–4613 (1994).
15. J. Moilanen, "New halo in Northern Finland," Weather **53,** 241–243 (1998).
16. C. Magono, S. Fujita, and T. Taniguchi, "Unusual type of single ice crystals originating from frozen cloud droplets," J. Atmos. Sci. **36,** 2495–2501 (1979).